Desalination and Water Treatment
www.deswater.com
doi: 10.1080/19443994.2015.1049409

57 (2016) 9027–9033
April

Taylor & Francis
Taylor & Francis Group

Fabrication, characterization and photocatalytic performance of Fe-doped TiO_2 nanotube composite for efficient degradation of water pollutants

Sung-Pil Kim, Jong-Oh Kim*

Department of Civil and Environmental Engineering, Hanyang University, 222 Wangsimni-ro, Seongdong-gu, Seoul 133-791, Korea, Fax: +82 2 2220 1945; email: jk120@hanyang.ac.kr (J.-O. Kim)

Received 9 February 2015; Accepted 15 April 2015

ABSTRACT

Pure TiO_2 nanotube and Fe-doped TiO_2 nanotube composite were fabricated by the electrochemical anodic oxidation process and the impregnating-calcination method, respectively. The structural and spectral properties were characterized by scanning electron microscopy, energy dispersive X-ray spectrometer, X-ray diffraction, Fourier transform infrared spectroscopy, photoluminescence, and UV–vis spectrum. These results showed that Fe was effectively deposited on the surface of TiO_2 nanotube. It is demonstrated that the Fe-doped TiO_2 nanotube composite can inhibit the recombination of electron–hole pairs and enhance the light harvesting ability. The photocatalytic activity of Fe-doped TiO_2 nanotube composite under UV irradiation was examined in terms of color and UV–vis absorbance for the degradation of methyl orange. The photocatalytic performance of UV-C irradiation in presence of Fe-doped TiO_2 nanotube composite increased obviously for the removal efficiency of color and UV–vis absorbance compared to that of UV-A irradiation, and the reaction rate constant was about 6.8 times faster than that of UV-A irradiation. This can be ascribed to the effective separation of the photo-generated charge carriers.

Keywords: TiO_2 nanotube; Anodic oxidation; Methyl orange; Doping; UV irradiation

1. Introduction

In the last decade, self-organized and vertically oriented TiO_2 nanotube arrays, first synthesized by Grimes and co-workers in 2001 [1], have attracted much attention due to their special and excellent properties such as highly ordered array structure, high specific surface areas, outstanding mechanical and chemical stability, and eminent charge-transfer properties [2,3]. TiO_2 nanotube has recently played an increased role in many practical fields, such as photodegradation of organic compounds [4], photoelectrolysis of water splitting [5], dye-sensitized solar cells [6], and hydrogen storage [7]. Despite these advantages, the efficiency of the photocatalytic degradation is limited by the high recombination rate of photo-generated electrons and holes due to its wide band gap (3.2 eV for anatase and 3.0 eV for rutile). To overcome this drawback, various methods have been studied including the substitutional non-metallic doping such as carbon [8], sulfur [9], fluorine [10], and

*Corresponding author.

Presented at IWA Regional Conference on Water Reuse and Energy 2014, 21–24 October 2014, Daegu, Korea

1944-3994/1944-3986 © 2015 Balaban Desalination Publications. All rights reserved.

nitrogen [11] as well as metal elements, such as iron [12], silver [13], platinum [14], and Aurum [15].

Among the various dopants, Fe is one of the most suitable for industrial applications considering its low cost and easy preparation. Doping TiO_2 with Fe^{3+} is an effective approach to reduce electron–hole recombination rate and increase photocatalytic efficiency in terms of its semi-full electronic configuration and ion radius close to Ti^{4+}. Many efforts have focused on the preparation and photocatalytic behavior of Fe^{3+}-doped TiO_2 nanoparticle powders or films [16], but few reports have so far been found regarding Fe^{3+}-doped TiO_2 nanotube [17,18]. These studies reported the improvement of photocatalytic activity under both visible light and UV light irradiation. It was commonly demonstrated that the improvement of photocatalysts was attributed to the Fe^{3+} dopant which can help the separation of photo-generated electrons and holes, and also can absorb and utilize the visible light to photocatalyze the degradation of pollutants [19].

In this study, Fe-doped TiO_2 nanotube composite was fabricated by the impregnating-calcination method using the prepared TiO_2 nanotube as precursors and $Fe(NO_3)_3{\cdot}9H_2O$ as dopant. Photocatalytic degradation of methyl orange (MO) under UV irradiation was investigated in terms of color and UV–vis absorbance. Effect of UV lamp types used in this experiment was also investigated with Fe-doped TiO_2 nanotube and pure TiO_2 nanotube. And, the structural and spectral properties of Fe-doped TiO_2 nanotube composite was characterized by scanning electron microscopy (SEM), energy dispersive X-ray spectrometer (EDS), X-ray diffraction (XRD), Fourier transform infrared spectroscopy (FT-IR), photoluminescence (PL), and UV–vis spectrum.

2. Experimental

2.1. Preparation of TiO_2 nanotube

TiO_2 nanotube on Ti substrate was prepared directly by the electrochemical anodic oxidation process (anodization method). All the anodization experiments were carried out at room temperature by a commercial available Ti foil (99.5% purity, 0.5 mm thickness) as the working electrode, a standard Pt foil as the counter electrode. Before anodization, Ti foil was degreased by sonication in acetone, ethanol, and deionized (DI) water for 30 min. Then, Ti foil was pre-anodized in ethylene glycol (EG) electrolyte composed of 0.15 M NH_4F and DI water at 60 V for 5 min. After anodization, TiO_2 nanotube was rinsed with distilled water and dried in the air to wipe off the debris on the surface of TiO_2 nanotube. Then, TiO_2 nanotube samples were annealed at 450℃ for 30 min in air.

2.2. Fabrication of Fe-doped TiO_2 nanotube composite

Fe-doped TiO_2 nanotube was prepared by an impregnating-calcination method using the as-prepared TiO_2 nanotube. The Fe source, used for the doping of Fe on the surface of TiO_2 nanotube, was 0.015 M $Fe(NO_3)_3{\cdot}9H_2O$ solution which was stirred continuously by a magnetic stirrer with heating (at 35℃) for 2 h. TiO_2 nanotube sample was mixed with 100 mL of 0.015 M $Fe(NO_3)_3{\cdot}9H_2O$ aqueous solution. In order to eliminate the effect of pH, the pH values of all mixed solutions were adjusted to 5 with a 0.1 M nitric acid solution. The mixed suspensions were stirred for 0.5 h, and then placed at room temperature for 24 h. After that, the mixed solution was dried in oven at 60℃ for 2 h and then washed with DI water. Finally, the samples were annealed at 300℃ for 2 h to get the Fe-doped TiO_2 nanotube. The detailed procedure to prepare the Fe-doped TiO_2 nanotube composite is shown in Fig. 1.

2.3. Characterization of pure TiO_2 nanotube and Fe-doped TiO_2 nanotube composite

The structural characterizations of the samples were carried out using field emission scanning electron microscopy (FE-SEM, Hitachi SU-70) equipped with an energy dispersive EDS. The crystal structure of pure TiO_2 nanotube and Fe-doped TiO_2 nanotube was examined by XRD (PANalytical X'pert PRO). The spectral characterizations of the samples were analyzed by FT-IR (Bruker Optics Vertex 80 & Hyperion 3000) and photoluminescence (PL, Hitachi F-7000, High S/N ratio of 250 (peak to peak), wavelength 480–540 nm). The absorption spectra were recorded by UV–vis spectroscopy (UV–vis NIR spectrophotometer, Hitachi U-4100).

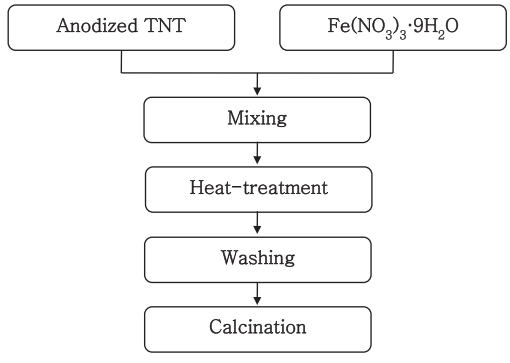

Fig. 1. A schematic procedure to prepare the Fe-doped TiO_2 nanotube composite.

2.4. Photocatalytic degradation of MO

The photocatalytic performance of Fe-doped TiO_2 nanotube was evaluated by degradation of MO as a target pollutant. All the experiments were performed in a 300-mL cylindrical glass reactor at a controlled temperature of 25°C. As UV lamps, UV-A (352 nm) type and UV-C (254 nm) type were used for photocatalytic activity. The sheet of Fe-doped TiO_2 nanotube with an area of approximately 4 $cm^2 \times 4$ was soaked in 200 mL MO (the concentration of 1 ppm) solution to achieve the degradation by UV irradiation. Color and UV–vis absorbance of MO samples were analyzed periodically using a DR-2010 (HACH) and spectrophotometer (Analytik Jena, SPECORD 50) by withdrawing small aliquots (25 mL) every 10 min. The relative absorbance of MO by UV–vis spectrophotometer was determined at 465 nm. After each analysis, the sample solution was returned back to the photo-reactor. The samples were used several times to test the repeatability of their photocatalytic performance. All the data presented here have been analyzed at least twice.

3. Results and discussion

3.1. Structural characterization of pure TiO_2 nanotube and Fe-doped TiO_2 nanotube

TiO_2 nanotube was prepared by anodization using an electrolyte composed of EG, 0.15 M NH_4F, and DI water at 60 V for 5 min. The SEM images of pure TiO_2 nanotube are shown in Fig. 2(a) and (b). It was clearly seen that the self-organized TiO_2 nanotube consists of a compact array of vertically gained nanotubes. The mean tube diameter and length of pure TiO_2 nanotube were about 74.5 nm and 5.13 μm, respectively. After the dipping process, TiO_2 nanotube was annealed at 300°C for 2 h and then Fe-doped TiO_2 nanotube was finally formed, as shown in Fig. 2(c). In Fig. 2(c), it can be seen that Fe is successfully deposited on the surface of TiO_2 nanotube. However, it can be seen that Fe deposits aggregate at the surface of TiO_2 nanotube and nanopores were partially clogged by them. In order to analyze chemical composition of Fe-doped TiO_2 nanotube composite, EDS result is indicated in Fig. 2(d). It demonstrated that EDS of Fe-doped TiO_2 nanotube composite exhibited the presence of Fe element in the bulk of the TiO_2 nanotube besides Ti and O, which was composed of elements, 32.69 At% Ti, 57.62 At% O, and 7.64 At% Fe.

XRD analysis was used to identify the phase structure and determine the crystallite size of samples. The XRD patterns of pure TiO_2 nanotube and Fe-doped TiO_2 nanotube are shown in Fig. 3. Peaks, marked "A" and "T" in Fig. 3, correspond to anatase phase and Ti, respectively. The diffraction peaks located at $2\theta = 25.31^\circ$, 37.03°, 37.93°, 38.39°, 47.95°, 54.00°, 55.00°, and 62.94° were correspondingly attributed to (101), (103), (004), (112), (200), (105), (211), and (204) planes of anatase TiO_2, respectively [17,18]. Fe diffraction peaks are not found in the XRD patterns. The absence of Fe diffraction peaks, even at 7.64 At% Fe, indicates that iron oxide may be highly dispersed on the surface of TiO_2 nanotube. It was reported that both Fe^{3+} (0.64 Å) and Ti^{4+} (0.68 Å) have similar ionic radius values; therefore, the Fe^{3+} ions can enter into the crystal structure of titania and locate at interstices or occupy some of the lattice sites of TiO_2, forming an iron–titanium solid solution [20].

3.2. Spectral characterization of pure TiO_2 nanotube and Fe-doped TiO_2 nanotube

FT-IR spectroscopy has been extensively used for identifying the various functional groups on the TiO_2 nanotube itself, as well as for identifying the adsorbed species and reaction intermediates on the surface of TiO_2 nanotube. Fig. 4 shows the FT-IR spectra of pure TiO_2 nanotube and Fe-doped TiO_2 nanotube. A FT-IR spectrum of pure TiO_2 nanotube shows a vibrational peak at 2,931 and 1920 cm^{-1}, respectively, which is attributed to bending vibration of hydroxyl groups present on the TiO_2 nanotube surface. The band at 1,023 cm^{-1} represents the stretching vibration of Ti–O bond, and band at 815 cm^{-1} is due to the Ti–O–Ti vibrational band of TiO_2 nanotube. In Fe-doped TiO_2 nanotube, the hydroxyl group peaks appeared at 3,046 and 2,248 cm^{-1}, respectively. The band at 927 and 821 cm^{-1} still exist in Fe-doped TiO_2 nanotube corresponding to Ti–O bond and Ti–O–Ti vibrational band of pure TiO_2 nanotube, respectively. Moreover, the intensity of these bands is stronger in case of TiO_2 nanotube with Fe content of 7.64 At% (Fig. 2(d)) than that of TiO_2 nanotube. This may be ascribed to be associated with the presence of Fe in the titania structure. And the band observed at 1,481 cm^{-1} is attributed to the vibration of molecular water bending mode.

UV–vis diffuse reflectance spectra were performed to test the light-harvesting capability of pure TiO_2 nanotube and Fe-doped TiO_2 nanotube. Fig. 5 shows the UV–vis diffuse reflectance spectra of pure TiO_2 nanotube and Fe-doped TiO_2 nanotube. In general, the light absorption characteristic of TiO_2 nanotube is affected by the presence of metal ions. A significant increase in the absorption at wavelengths longer than 380 nm was observed for the Fe-doped TiO_2 nanotube.

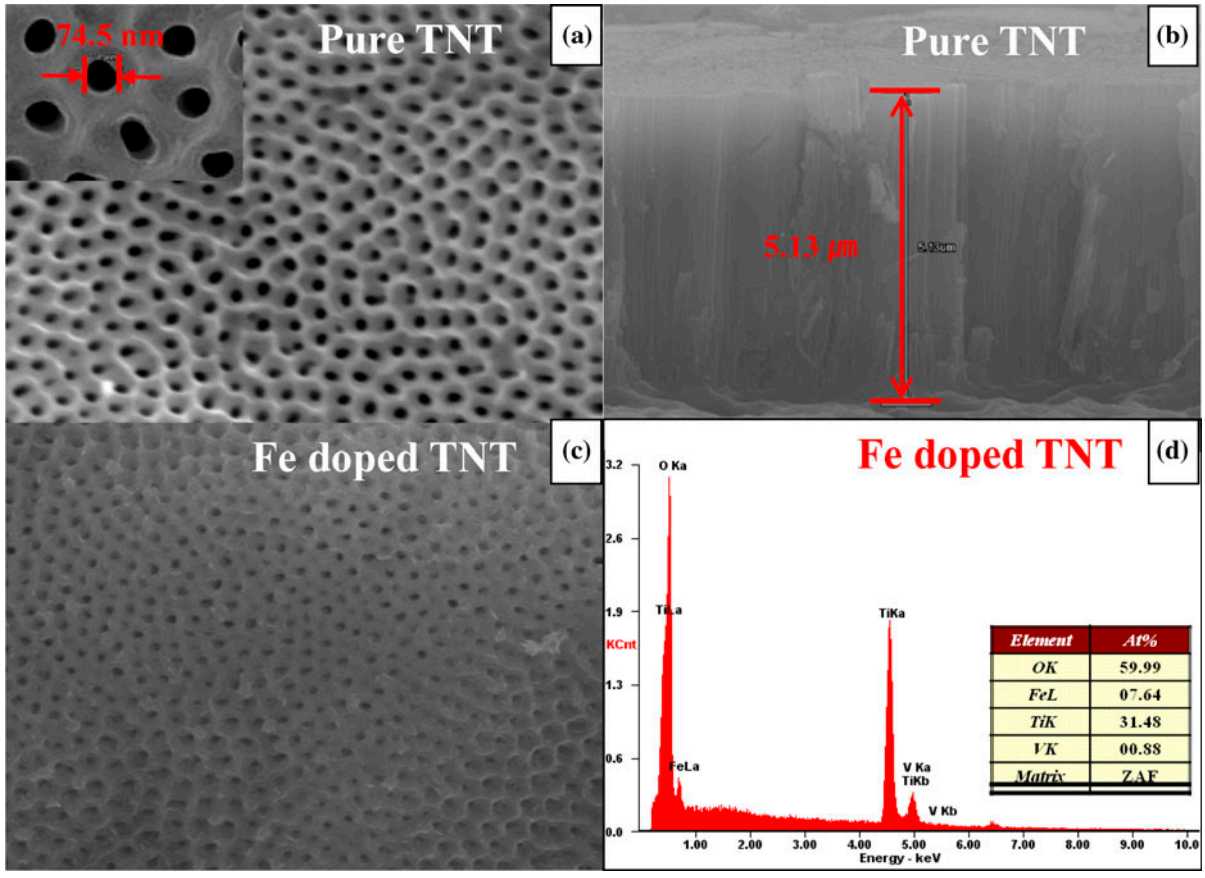

Fig. 2. SEM images of top (a) and cross-sectional (b) views of pure TiO_2 nanotube, top view of Fe-doped TiO_2 nanotube (c), EDS of Fe-doped TiO_2 nanotube (d).

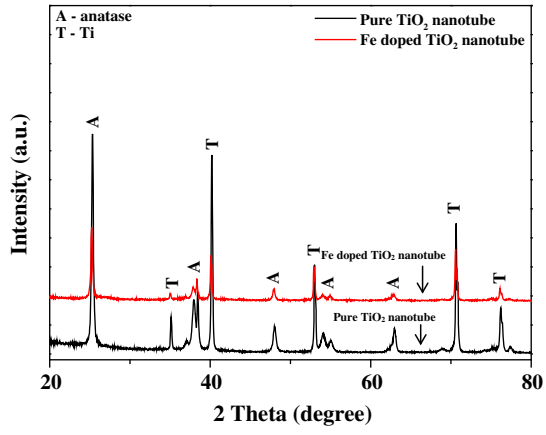

Fig. 3. XRD patterns of pure TiO_2 nanotube and Fe-doped TiO_2 nanotube.

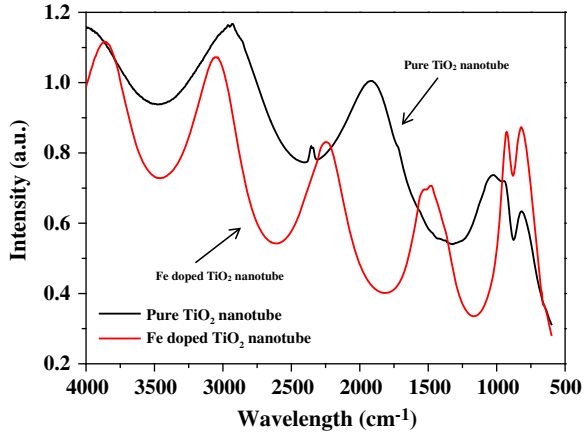

Fig. 4. FT-IR spectra of pure TiO_2 nanotube and Fe-doped TiO_2 nanotube.

The spectrum of Fe-doped TiO_2 nanotube showed a strong absorption in the visible light region and was red shifted compared to the spectrum of TiO_2 nanotube. Red shift associated with the presence of Fe ions could be attributed to a charge transfer transition between Fe ions electrons and TiO_2 conduction or

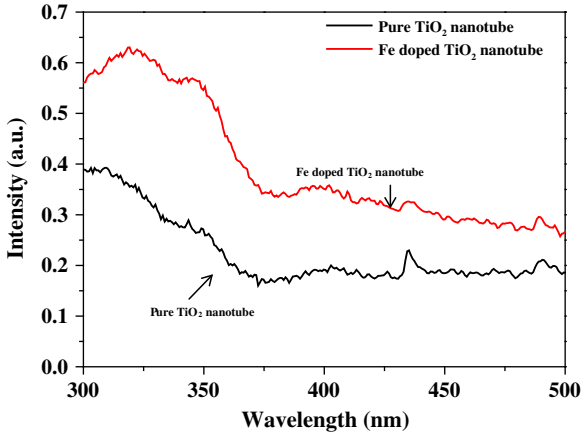

Fig. 5. UV–vis diffuse reflectance spectra of pure TiO_2 nanotube and Fe-doped TiO_2 nanotube.

valence bands, which facilitate the absorption of the abundant visible light [21].

It is well known that photocatalytic activity is closely related with the lifetime of photo-generated electrons and holes [22]. The separation and recombination processes of photo-generated charge carriers in nanosized semiconductor materials could be reflected by PL spectrum. Thus, PL spectrum could provide a firm foundation for a quick evaluation of the photocatalytic activity of semiconductor samples [23]. Fig. 6 shows the PL spectra of pure TiO_2 nanotube and Fe-doped TiO_2 nanotube to confirm the photo-generated charge separation and recombination behaviors. The excitation wavelength of samples was 341 nm and the spectra were monitored in the range of 350–500 nm. As shown in Fig. 6, pure TiO_2 nanotube and Fe-doped TiO_2 nanotube are similar to the same position of emission peak, whereas PL intensity of Fe-doped TiO_2 nanotube was lower than that of pure TiO_2 nanotube. The weaker intensity of Fe-doped TiO_2 nanotube than that of pure TiO_2 nanotube shown in Fig. 6 is due to the doping of Fe which allows more efficient light harvesting and results in an increase in the quantity of photo-generated charge carriers. Consequentially, it indicated that the recombination of photo-induced electron–hole pairs in Fe-doped TiO_2 nanotube composite was inhibited effectively.

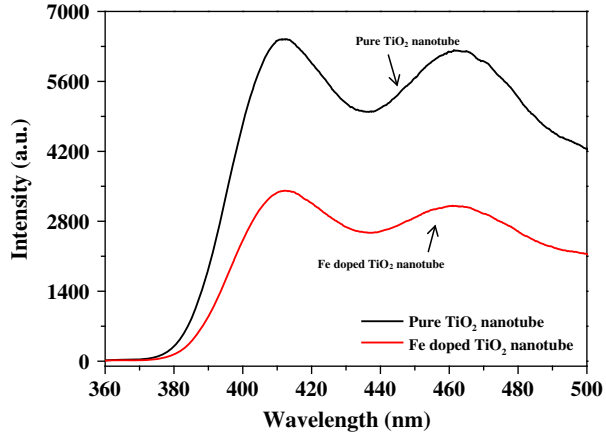

Fig. 6. PL spectra of pure TiO_2 nanotube and Fe-doped TiO_2 nanotube.

3.3. Photocatalytic activity of Fe-doped TiO_2 nanotube

MO was used as a model target pollutant to investigate the photocatalytic activity of Fe-doped TiO_2 nanotube under UV irradiation. Fig. 7(a) shows the reaction rate of MO in the presence of the Fe-doped TiO_2 nanotube under UV irradiation of 32 W at two different UV lamp types. It is noted that the plot of $\ln(C/C_0)$ vs. illumination time represents a

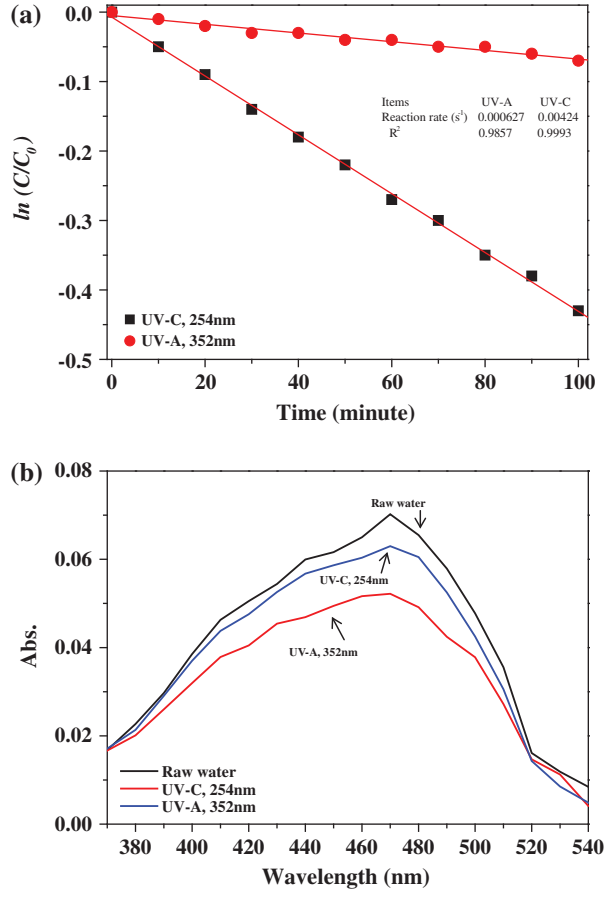

Fig. 7. (a) photodegradation rate and (b) UV–vis absorbance of Fe-doped TiO_2 nanotube composite at two different UV lamp types for the degradation of MO.

straight line and the slope of linear regression can be equal to the apparent first-order rate constant. The first-order rate constant and correlation coefficient (R^2) of UV-C and UV-A irradiation were about 0.00424 s^{-1} and 0.9993, and about 0.000627 s^{-1} and 0.9857, respectively. The reaction rate constant of UV-C irradiation was about 6.8 times faster than that of UV-A irradiation. This may be ascribed to the more effective separation of the photo-generated electron–hole pairs, thus inhibiting the recombination of the photo-induced electrons and holes and leading to an increase in the concentration of the photo-generated charge carrier [17]. Fig. 7(b) shows the UV–vis absorbance of MO degraded by the Fe-doped TiO_2 nanotube at two different UV lamp type. It is observed that the absorption peak of MO was the wavelength of 465 nm. The lowest absorbance of MO photodegradation was indicated in UV-C irradiation in the presence of Fe-doped TiO_2 nanotube composite after irradiation time of 100 min. When Fe-doped TiO_2 nanotube in MO solution is irradiated by UV light, an electron may be excited from the valence band to the conduction band leaving behind an electron vacancy (hole) in the valence band (Eq. (1)). Fe^{3+} can trap photo-generated holes (Eq. (2)) due to the energy levels for Fe^{4+}/Fe^{3+} (2.20 V vs. normal hydrogen electrode) above the valence band edge of anatase TiO_2 [21]. The trapped holes in Fe^{4+} can migrate to the surface and absorb hydroxyl ion to produce hydroxyl radical (Eq. (3)). Simultaneously, Fe^{3+} also traps photo-generated electrons (Eq. (4)) due to the energy level for Fe^{3+}/Fe^{2+} (0.771 V vs. normal hydrogen electrode) below the conductor band edge of TiO_2, which has been supported by EPR results [21]. Subsequently, Fe^{2+} could be oxidized to Fe^{3+} by transferring electrons to absorbed O_2 on the surface of TiO_2 (Eq. (5)). When Fe-doped TiO_2 nanotube is irradiated by UV light, the main reactions can be expressed as follows [24].

As has been described above, the Fe doping leads to enhanced absorption in Fe-doped TiO_2 nanotubes and narrowing of the band gap of TiO_2 by introducing a doping energy level.

$$TNT + h\nu \rightarrow e^- + h^+ \quad (1)$$

$$Fe^{3+} + h^+ \rightarrow Fe^{4+} \quad (2)$$

$$Fe^{4+} + OH^- \rightarrow Fe^{3+} + OH^{\cdot} \quad (3)$$

$$Fe^{3+} + e^- \rightarrow Fe^{2+} \quad (4)$$

$$Fe^{2+} + O_2 \rightarrow Fe^{3+} + O_2^- \quad (5)$$

4. Conclusions

TiO_2 nanotube doped with the content of 7.64 At% Fe was prepared by an impregnating-calcination method using TiO_2 nanotube as the precursor and Fe $(NO_3)_3{\cdot}9H_2O$ as the dopant. The Fe-doped TiO_2 nanotube composite was evaluated by the structural and spectral properties as well as the photocatalytic activity. The results of the structural and spectral property (SEM, EDS, XRD, FT-IR, PL, and UV–vis spectrum) showed that Fe was effectively deposited on the surface of TiO_2 nanotube. It reveals that the Fe-doped TiO_2 nanotube composite can inhibit the recombination of electron–hole pairs and enhance the adsorption performance both in the UV light range and the visible-light range. The enhanced photocatalytic performance of Fe-doped TiO_2 nanotube composite in presence of UV irradiation was observed in UV-C lamp. The reaction rate constant of UV-C irradiation was about 6.8 times faster than that of UV-A irradiation. This can be ascribed to the effective separation of the photo-generated charge carriers.

Acknowledgments

This study was supported by a National Research Foundation of Korea (NRF) grant funded by the Korean Government (NRF-2013R1A2A1A09007252).

References

[1] D. Gong, C. Grimes, O. Varghese, W. Hu, R. Singh, Z. Chen, E. Dickey, Titanium oxide nanotube arrays prepared by anodic oxidation, J. Mater. Res. 16 (2001) 3331–3334.
[2] A. Maurya, P. Chauhan, Structural and optical characterization of CdS/TiO_2 nanocomposite, Mater. Charact. 62 (2011) 382–390.
[3] K. Xie, L. Sun, C. Wang, Y. Lai, M. Wang, H. Chen, C. Lin, Photoelectrocatalytic properties of Ag nanoparticles loaded TiO_2 nanotube arrays prepared by pulse current deposition, Electrochim. Acta 55 (2010) 7211–7218.
[4] S. Albu, A. Ghicov, J. Macak, R. Hahn, P. Schmuki, Self-organized, free-standing TiO_2 nanotube membrane for flow-through photocatalytic applications, Nano. Lett. 7 (2007) 1286–1289.
[5] J. Gong, Y. Lai, C. Lin, Electrochemically multi-anodized TiO_2 nanotube arrays for enhancing hydrogen generation by photoelectrocatalytic water splitting, Electrochim. Acta 55 (2010) 4776–4782.
[6] J. Yan, F. Zhou, TiO_2 nanotubes: Structure optimization for solar cells, J. Mater. Chem. 21 (2011) 9406–9418.
[7] A. Mishra, S. Banerjee, S. Mohapatra, O. Graeve, M. Misra, Synthesis of carbon nanotube–TiO_2 nanotubular material for reversible hydrogen storage, Nanotechnology 19 (2008) 445–607.

[8] A. Morawski, M. Janus, B. Tryba, M. Toyoda, T. Tsumura, M. Inagaki, Carbon modified TiO_2 photocatalysts for water purification, Pol. J. Chem. Technol. 11 (2009) 46–50.
[9] T. Ohno, M. Akiyoshi, T. Umebayashi, K. Asai, T. Mitsui, Preparation of S-doped TiO_2 photocatalysts and their photocatalytic activities under visible light, Appl. Catal. A-Gen. 265 (2004) 115–121.
[10] H. Jiang, H. Song, Z. Zhou, X. Liu, G. Meng, Characterization of LiF-doped TiO_2 and its photocatalytic activity for decomposition of trichloromethane, Mater. Res. Bull. 43 (2008) 3037–3046.
[11] Z. Zhang, X. Wang, J. Long, Q. Gu, Z. Ding, X. Fu, Nitrogen-doped titanium dioxide visible light photocatalyst: Spectroscopic identification of photoactive centers, J. Catal. 276 (2010) 201–214.
[12] H. Yu, H. Irie, Y. Shimodaira, Y. Hosogi, Y. Kuroda, M. Miyauchi, K. Hashimoto, An efficient visible-light-sensitive Fe(III) grafted TiO_2 photocatalyst, J. Phys. Chem. C 114 (2010) 16841–16847.
[13] S. Chen, M. Malig, M. Tian, A. Chen, Electrocatalytic activity of PtAu nanoparticles deposited on Tio_2 nanotubes, J. Phys. Chem. C 116 (2012) 3298–3304.
[14] E. Stathatos, T. Petrova, P. Lianos, Study of the efficiency of visible-light photocatalytic degradation of basic blue adsorbed on pure and doped mesoporous titania films, Langmuir 17 (2001) 5025–5030.
[15] M. Tian, G. Wu, A. Chen, Unique electrochemical catalytic behavior of Pt nanoparticles deposited on TiO_2 nanotubes, ACS Catal. 2 (2012) 425–432.
[16] T. Tong, J. Zhang, B. Tian, F. Chen, D. He, Preparation of Fe^{3+}-doped TiO_2 catalysts by controlled hydrolysis of titanium alkoxide and study on their photocatalytic activity for methyl orange degradation, J. Hazard. Mater. 155 (2008) 572–579.
[17] X. Wei, H. Wang, G. Zhu, J. Chen, L. Zhu, Iron-doped TiO_2 nanotubes with high photocatalytic activity under visible light synthesized by an ultrasonic-assisted sol-hydrothermal method, Ceram. Int. 39 (2013) 4009–4016.
[18] Q. Wu, J. Ouyang, K. Xie, L. Sun, M. Wang, C. Lin, Ultrasound-assisted synthesis and visible-light-driven photocatalytic activity of Fe-incorporated TiO_2 nanotube array photocatalysts, J. Hazard. Mater. 199–200 (2012) 410–417.
[19] J. Yu, Q. Xiang, M. Zhou, Preparation, characterization and visible-light-driven photocatalytic activity of Fe-doped titania nanorods and first-principles study for electronic structures, Appl. Catal., B 90 (2009) 595–602.
[20] K. Narasimharao, M. Malik, M. Mokhtar, S. Basahel, S. Al-Thabaiti, Iron oxide supported sulfated TiO_2 nanotube catalysts for NO reduction with propane, Ceram. Int. 40 (2014) 4039–4053.
[21] J. Zhu, W. Zheng, B. He, J. Zhang, M. Anpo, Characterization of Fe-TiO_2 photocatalysts synthesized by hydrothermal method and their photocatalytic reactivity for photodegradation of XRG dye diluted in water, J. Mol. Catal. A: Chem. 216 (2004) 35–43.
[22] H. Zhao, H. Li, H. Yu, H. Chang, X. Quan, S. Chen, CNTs–TiO_2/Al_2O_3 composite membrane with a photocatalytic function: Fabrication and energetic performance in water treatment, Sep. Purif. Technol. 116 (2013) 360–365.
[23] L. Jing, Y. Qu, B. Wang, S. Li, B. Jiang, L. Yang, W. Fu, H. Fu, J. Sun, Review of photoluminescence performance of nano-sized semiconductor materials and its relationships with photocatalytic activity, Sol. Energy Mater. Sol. Cells 90 (2006) 1773–1787.
[24] Y. Pang, A. Abdullah, Fe^{3+} doped TiO_2 nanotubes for combined adsorption–sonocatalytic degradation of real textile wastewater, Appl. Catal., B 129 (2013) 473–481.